TWIN TAIL/DELTA WING CONFIGURATION BUFFET DUE TO
UNSTEADY VORTEX BREAKDOWN FLOW

NDE

NA-/- 6-7-8

/N -)S -

034 379

Osama A. Kandil[1] , Essam F. Sheta[2] and Steven J. Massey[3]
Aerospace Engineering Department
Old Dominion University, Norfolk, VA 23529-0247

ABSTRACT

The buffet response of the twin-tail configuration of the F/A-18 aircraft; a multidisciplinary problem, is investigated using three sets of equations on a multi-block grid structure. The first set is the unsteady, compressible, full Navier-Stokes equations. The second set is the coupled aeroelastic equations for bending and torsional twin-tail responses. The third set is the grid-displacement equations which are used to update the grid coordinates due to the tail deflections. The computational model consists of a 76°-swept back, sharp edged delta wing of aspect ratio of one and a swept-back F/A-18 twin-tails. The configuration is pitched at 32° angle of attack and the freestream Mach number and Reynolds number are 0.2 and 0.75 x 10^6, respectively. The problem is solved for the initial flow conditions with the twin tail kept rigid. Next, the aeroelastic equations of the tails are turned on along with the grid-displacement equations to solve for the uncoupled bending and torsional tails response due to the unsteady loads produced by the vortex breakdown flow of the vortex cores of the delta wing. Two lateral locations of the twin tail are investigated. These locations are called the midspan and inboard locations.

INTRODUCTION

The ability of modern combat aircraft to fly and maneuver at high angles of attack and at high loading conditions is of prime importance. This capability is achieved, for example in the F/A-18 fighter, through the combination of the leading-edge extension (LEX) with a delta wing and the use of vertical tails. The LEX maintains lift at high angles of attack by generating a pair of vortices that trail aft over the top of the aircraft. The vortex entrains air over the vertical tails to maintain stability of the aircraft. This combination of LEX, delta wing and vertical tails leads to the aircraft excellent agility. However, at some flight conditions, the vortices emanating from the highly-swept LEX of the delta wing breakdown before reaching the vertical tails which get bathed in a wake of unsteady highly-turbulent, swirling flow. The vortex-breakdown flow produces unsteady, unbalanced loads on the vertical tails which in turn produce severe buffet of the tails and has led to their premature fatigue failure.

Experimental investigation of the vertical tail buffet of the F/A-18 models have been conducted by several investigators such as Sellers at al[1]., Erickson at al[2]., Wentz[3] and Lee and Brown[4]. These experiments showed that the vortex produced by the LEX of the wing breaks down ahead of the vertical tails at angles of attack of 25° and higher and the breakdown flow produced unsteady loads on the vertical tails. Rao, Puram and Shah[5] proposed two aerodynamic concepts for alleviating high-alpha tail buffet characteristics of the twin tail fighter configurations. Cole, Moss and Doggett[6] tested a rigid, 1/6 size, full-span model of an F-18 airplane that was fitted with flexible vertical tails of two different stiffness. Vertical-tail buffet response results were obtained over the range of angle of attack from −10° to +40°, and over the range of Mach numbers from 0.3 to 0.95. Their results indicated that the buffet response occurs in the first bending mode, increases with increasing dynamic pressure and is larger at $M = 0.3$ than that at a higher Mach number.

---

[1] Professor, Eminent Scholar and Chair of Aerospace Engineering Dept., AIAA Associate Fellow.
[2] Ph.D. Graduate Research Assistant, Aerospace Engineering Dept., Member AIAA.
[3] Ph.D. Graduate Research Assistant, Aerospace Engineering Dept., Member AIAA.

An extensive experimental investigation has been conducted to study vortex-fin interaction on a 76° sharp-edged delta wing with vertical twin-fin configuration by Washburn, Jenkins and Ferman[7]. The vertical tails were placed at nine locations behind the wing. The experimental data showed that the aerodynamic loads are more sensitive to the chordwise tail location than its spanwise location. As the tails were moved toward the vortex core, the buffeting response and excitation were reduced. Although the tail location did not affect the vortex core trajectories, it affected the location of vortex-core breakdown. Moreover, the investigation showed that the presence of a flexible tail can affect the unsteady pressures on the rigid tail on the opposite side of the model. In a recent study by Bean and Lee[8] tests were performed on a rigid 6% scale F/A-18 in a trisonic blowdown wind tunnel over a range of angle of attack and Mach number. The flight data was reduced to a non-dimensional buffet excitation parameter, for each primary mode. It was found that buffeting in the torsional mode occurred at a lower angle of attack and at larger levels compared to the fundamental bending mode.

Kandil, Kandil and Massey[9] presented the first successful computational simulation of the vertical tail buffet using a delta wing-vertical tail configuration. A 76° sharp-edged delta wing has been used along with a single rectangular vertical tail which was placed aft the wing along the plane of geometric symmetry. The tail was allowed to oscillate in bending modes. The flow conditions and wing angle of attack have been selected to produce an unsteady vortex-breakdown flow. Unsteady vortex breakdown of leading-edge vortex cores was captured, and unsteady pressure forces were obtained on the tail. These computational results are in full qualitative agreement with the experimental data of Washburn, Jenkins and Ferman[7].

Kandil, Kandil and Massey[10] extended the technique used in Ref. 9 to allow the vertical tail to oscillate in both bending and torsional modes. The total deflections and the frequencies of deflections and loads of the coupled bending-torsion case were found to be one order of magnitude higher than those of the bending case only. Also, it has been shown that the tail oscillations change the vortex breakdown locations and the unsteady aerodynamic loads on the wing and tail.

Kandil, Massey and Sheta[11] studied the effects of coupling and uncoupling the bending and torsional modes for a long computational time, and the flow Reynolds number on the buffet response, of a single rectangular tail. It has been shown that the coupled response produces higher deflection than that of the uncoupled response. Moreover, the response of the coupled case reaches periodicity faster than that of the uncoupled case. It has also been shown that the deflections of the low-Reynolds number case are substantially lower than that of the high Reynolds number case.

In a very recent paper by Kandil, Sheta and Massey[12], the buffet response of a single swept-back vertical tail in transonic flow at two angles of attack (20°, 28°) has been studied. It has been shown that the aerodynamic loads and bending-torsional deflections of the tail never reached periodic response and that the loads are one order of magnitude lower than those of Ref. 11 of the subsonic flow.

In this paper, we consider the buffet response of the F/A-18 twin tail. The configuration consists of a 76°-swept back, sharp-edged delta wing and a T-extension on which the F/A-18 twin tail is attached as a cantilevers. A multi-block grid is used to solve the problem for two lateral locations of the twin tail; the midspan location and the inboard location.

FORMULATION

The formulation consists of three sets of governing equations along with certain initial and boundary conditions. The first set is the unsteady, compressible, full Navier-Stokes equations. The second set consists of the aeroelastic equations for bending and torsional modes. The third set consists of equations for deforming the grid according to the twin tail deflections. Next, the governing equations of each set along with the initial and boundary conditions are given.

Fluid-Flow Equations:

The conservative form of the dimensionless, unsteady, compressible, full Navier-Stokes equations in terms of time-dependent, body-conformed coordinates ξ^1, ξ^2 and ξ^3 is given by

$$\frac{\partial \bar{Q}}{\partial t} + \frac{\partial \bar{E}_m}{\partial \xi^m} - \frac{\partial (\bar{E}_v)_s}{\partial \xi^s} = 0; m = 1-3, s = 1-3 \quad (1)$$

where

$$\xi^m = \xi^m(x_1, x_2, x_3, t) \quad (2)$$

$$\bar{Q} = \frac{1}{J}[\rho, \rho u_1, \rho u_2, \rho u_3, \rho e]^t, \quad (3)$$

$\bar{E}_m$ and $(\bar{E}_v)_s$ are the ξ^m-inviscid flux and ξ^s-viscous and heat conduction flux, respectively. Details of these fluxes are given in Ref. 9.

Aeroelastic Equations:

The dimensionless, linearized governing equations for the coupled bending and torsional vibrations of a vertical tail that is treated as a cantilevered beam are considered. The tail bending and torsional deflections occur about an elastic axis that is displaced from the inertial axis. These equations for the bending deflection, w, and the twist angle, θ, are given by

$$\frac{\partial^2}{\partial z^2}\left[EI(z)\frac{\partial^2 w}{\partial z^2}(z,t)\right] + m(z)\frac{\partial^2 w}{\partial t^2}(z,t)$$

$$+ m(z)x_\theta(z)\frac{\partial^2 \theta}{\partial t^2}(z,t) = N(z,t) \quad (4)$$

$$\frac{\partial}{\partial z}\left[GJ(z)\frac{\partial \theta}{\partial z}\right] - m(z)x_\theta \frac{\partial^2 w}{\partial t^2}(z,t)$$

$$- I_\theta(z)\frac{\partial^2 \theta}{\partial t^2}(z,t) = -M_t(z,t) \quad (5)$$

where z is the vertical distance from the fixed support along the tail length, l_t, EI and GJ the bending and torsional stiffness of the tail section, m the mass per unit length, I_θ the mass-moment of inertia per unit length about the elastic axis, x_θ the distance between the elastic axis and inertia axis, N the normal force per unit length and M_t the twisting moment per unit length. The characteristic parameters for the dimensionless equations are c^*, a_∞^*, ρ_∞^* and c^*/a_∞^* for the length, speed, density and time; where c^* is the delta wing root-chord length, a_∞^* the freestream speed of sound and ρ_∞^* the freestream air density. The geometrical and natural boundary conditions on w and θ are given by

$$w(0,t) = \frac{\partial w}{\partial z}(0,t) = \frac{\partial^2 w}{\partial z^2}(l_t,t)$$

$$= \frac{\partial}{\partial z}\left[EI(l_t)\frac{\partial^2 w}{\partial z^2}(l_t,t)\right] = 0 \quad (6)$$

$$\theta(0,t) = \frac{\partial \theta}{\partial z}(l_t,t) = 0 \quad (7)$$

The solution of Eqs. (4) and (5) are given by

$$w(z,t) = \sum_{i=1}^{\bar{I}} \phi_i(z)q_i(t) \quad (8)$$

$$\theta(z,t) = \sum_{j=\bar{I}+1}^{M} \phi_j(z)q_j(t) \quad (9)$$

where ϕ_i and ϕ_j are comparison functions satisfying the free-vibration modes of bending and torsion, respectively, and q_i and q_j are generalized coordinates for bending and torsion, respectively. In this paper, the number of bending modes, $\bar{I}$, is six and the number of torsion modes, $M - \bar{I}$, is also six. Substituting Eqs. (8) and (9) into Eqs. (4) and (5) and using the Galerkin method along with integration by parts and the boundary conditions, Eqs (6) and (7), we get the following equation for the generalized coordinates q_i and q_j in matrix form:

$$\begin{bmatrix} M_{11} & M_{12} \\ M_{21} & M_{22} \end{bmatrix}\begin{pmatrix} \ddot{q}_i \\ \ddot{q}_j \end{pmatrix} + \begin{bmatrix} K_{11} & 0 \\ 0 & K_{22} \end{bmatrix}\begin{pmatrix} q_i \\ q_j \end{pmatrix}$$

$$= \begin{pmatrix} \hat{N}_1 \\ \hat{N}_2 \end{pmatrix} \begin{matrix} ; i = 1, 2, ..., \bar{I} \\ ; j = \hat{I}+1, ..., M \end{matrix} \quad (10)$$

where

$$\begin{aligned} M_{11} &= & \int_0^{l_t} m\phi_r\phi_i dz \\ M_{12} &= M_{21} = \int_0^{l_t} mx_\theta\phi_r\phi_j dz \\ M_{22} &= & \int_0^{l_t} I_\theta\phi_s\phi_j dz \end{aligned} \right\} \quad (11)$$

$$\begin{aligned} K_{11} &= \int_0^{l_t} EI\frac{d^2\phi_r}{dz^2}\frac{d^2\phi_i}{dz^2}dz \\ K_{22} &= \int_0^{l_t} GJ\frac{d\phi_s}{dz}\frac{d\phi_j}{dz}dz \end{aligned} \right\} \quad (12)$$

$$\begin{aligned} \hat{N}_1 &= \int_0^{l_t} \phi_r N dz \\ \hat{N}_2 &= \int_0^{l_t} \phi_s M_t dz \end{aligned} \right\} \quad (13)$$

Similar aeroelastic equations were developed for sonic analysis of wing flutter by Strganac[13]. The numerical integration of Eqs. (11-13) is obtained using the trapezoidal method with 125 points to improve the accuracy of integrations. The solution of Eq. (10), for $q_i; i = 1, 2, ..., \bar{I}$, and $q_j; j = \bar{I}+1, ..., M$, is obtained using the Runge-Kutta scheme. Next, w, and θ are obtained from Eqs. (8) and (9).

3

Grid Displacement Equations:

Once w and θ are obtained at the $n+1$ time step, the new grid coordinates are obtained using simple interpolation equations. In these equations, the twin tail bending displacements, $w^{n+1}_{i,j,k}$, and their displacement through the torsion angle, $\theta^{n+1}_{i,j,k}$ are interpolated through cosine functions.

Boundary and Initial Conditions:

Boundary conditions consists of conditions for the fluid flow and conditions for the aeroelastic bending and torsional deflections of the twin tail. For the fluid flow, the Riemann-invariant boundary conditions are enforced at the inflow and outflow boundaries of the computational domain. At the plane of geometric symmetry, periodic boundary conditions is specified with the exception of grid points on the tail. On the wing surface, the no-slip and no-penetration conditions are enforced and $\frac{\partial p}{\partial n} = 0$. On the tail surface, the no-slip and no-penetration conditions for the relative velocity components are enforced (points on the tail surface are moving). The normal pressure gradient is no longer equal to zero due to the acceleration of the grid points on the tail surface. This equation becomes $\frac{\partial p}{\partial n} = -\rho \bar{a}_t . \hat{n}$, where $\bar{a}_t$ is the acceleration of a point on the tail and $\hat{n}$ is the unit normal.

Initial conditions consist of conditions for the fluid flow and conditions for the aeroelastic deflections of the twin tail. For the fluid flow, the initial conditions correspond to the freestream conditions with no-slip and no-penetration conditions on the wing and tail. For the aeroelastic deflections of the tail, the initial conditions for any point on the tail are that the displacement and velocity are zero, $w(z,0) = 0$, $\frac{\partial w}{\partial t}(z,0) = 0$, $\theta(z,0) = 0$ and $\frac{\partial \theta}{\partial t}(z,0) = 0$.

METHOD OF SOLUTION

The first step is to solve for the fluid flow problem using the vortex-breakdown conditions and keeping the tail as a rigid beam. Navier-Stokes equations are solved using the implicit, flux-difference splitting finite-volume scheme. The grid speed $\frac{\partial \xi^m}{\partial t}$ is set equal to zero in this step. This step provides the flow field solution along with the pressure difference across the tail. The pressure difference is used to generate the normal force and twisting moment per unit length of the tail. Next, the aeroelastic equations are used to obtain the

twin tail deflections, $w_{i,j,k}$ and $\theta_{i,j,k}$. The grid displacement equations are then used to compute the new grid coordinates. The metric coefficient of the coordinate Jacobian matrix are updated as well as the grid speed, $\frac{\partial \xi^m}{\partial t}$. This computational cycle is repeated every time step.

COMPUTATIONAL APPLICATIONS AND DISCUSSION

Twin Tail-Delta Wing Configuration:

The twin tail-delta wing configuration consists of a 76°-swept back, sharp-edged delta wing (aspect ratio of one) and a F/A-18 twin tail. Each tail is of aspect ratio 1.2, a crop ratio of 0.4 and a sweepback angle of 35° for the quarter-chord spanwise line. The chord length at the root is 0.4 and at the tip is 0.159, with a span length of 0.336. The tail airfoil section is a NACA 65-A with sharp leading edge and the thickness ratio is 5% at the root and 3% at the tip. The dihedral angle between the two tails is 40°. The tails are cantilevered on the upper surface of a trailing-edge extension of the delta wing. The configuration is pitched at an angle of attack of 32° and the freestream Mach number and Reynolds number are 0.2 and 0.75 x 10^6; respectively.

A multi-block grid consisting of 4 blocks is used for the solution of the problem. The first block is a O-H grid for the wing and upstream region, with 101X50X54 grid points in the wrap around, normal and axial directions, respectively. The second block is a H-H grid for the inboard region of the twin tail, with 23X50X14 grid points in the wrap around, normal and axial directions, respectively. The third block is a H-H grid for the outboard region of the twin tail, with 79X50X14 grid points in the wrap around, normal and axial directions, respectively. The fourth block is a O-H grid for the downstream region of the twin tail, with 101X50X24 grid points in the wrap around, normal and axial directions, respectively. Figure 1 shows the grid topology and a blow-up of the twin tail-delta wing configuration.

The configuration is investigated for two spanwise separation distance between the twin tail; the mid-span location for which the separation distance is 56% of the wing span and the inboard location for which the separation distance is 33% of the wing span.

4

Mid-span Location of Twin Tail (56% wing span):
Initial Conditions:

Keeping the twin tail rigid, the unsteady, compressible, full Navier-Stokes equations are integrated time accurately using the implicit, flux-difference splitting scheme of Roe with a $\Delta t = 0.001$ to a dimensionless time, $t = 4.0$. Figure 2 shows three-dimensional views of the total pressure on the wing and twin tail surfaces, the vortex cores particle traces and the vortex cores iso-total pressure surfaces. Figure 3 shows the static-pressure contours and the instantaneous streamlines in a cross-flow plane which is located at $x = 1.133$. It is observed from Fig. 2 that the vortex-breakdown locations are forward of the wing trailing edge, about 72% of the wing chord (consistent with Washburn, et al results[7]), and their shape and locations are slightly asymmetric. Figure 3 shows that the vortex-breakdown flow is inside the region between the twin tail. It is also observed that a small vortex flow develops on the outside corner of the juncture of the tail and the trailing edge extension (consistent with Washburn, et al results[7]). The static pressure contours show a lower-pressure level over the inside surface of the tail than the pressure level over the outside surface of the tail.

Uncoupled Bending-Torsion Twin Tail Response:

Each of the tail is treated as a swept back beam with dimensionless modulii of elasticity and rigidity, E and G of $1.8 X 10^5$ and $0.692 X 10^5$; respectively. The density ratio, (ρ/ρ_∞), of the tail material is taken as 32. For the present cases of uncoupled bending-torsion response, the distance between the elastic axis and the inertia axis, x_θ, in Eqs. (4) and (5) is set equal to zero.

Figure 4-11 show the fluid flow and structural responses of the this case. Figure 4 and 5 show the three dimensional views and the cross-flow plane views at $x = 1.133$ and $it = 6,000$ time steps ($t = 6.0$) after the initial conditions. Figure 4 shows that the vortex breakdown locations have moved forward of the vortex-breakdown locations of the initial conditions. Figure 5 shows that the vortex-breakdown flow is still inside the region between the twin tail, asymmetric and experiencing more breakdown in comparison of the initial conditions results of Fig. 3. The static pressure contours inside the region between the twin tail of Fig. 5 show higher pressure levels than those of the initial conditions results of Fig. 3. It is conclusively evident that the deflections of the twin tail change the locations and shapes of the vortex breakdown flow on the wing and between the twin tail.

The structural responses of the twin tail show interesting results which are used to explain the fluid flow responses. These results are given in Figs. 6-11 with Figs. 6, 8 and 10 for the right tail (as viewed in the upstream direction) and with Figs. 7,9 and 11 for the left tail. Figures 6 and 7 show the distributions of deflections and loads for bending and torsion responses of the right and left tails along the vertical distance z every 1000 time steps. It is observed that the bending responses are in the first mode shape while the torsion responses are combinations of the first, second and third mode shapes. Moreover, the maximum bending deflections are about two times those of the torsion deflections. Figure 8 and 9 show the history of the bending and torsion deflections and loads versus time of the tail tip point and the mid point. Within the range of computational time (10,000 time steps = 10 time units), the bending oscillations of the tail tips are damped with an approximate mean value of $w = -6 X 10^{-4}$ (right tail) and $+6 X 10^{-4}$ (left tail). In the meantime, the torsion deflections at the tip are increasing with time with the right tail showing opposite sign of deflection angles in comparison with the left tail. Figures 10 and 11 show the total deflection (bending plus torsion) distribution along the vertical distance z every 1000 time steps and the history of the root bending moment versus time for the right and left tails. It is observed that the total deflection distributions for the right and left tails are of opposite sign and the same observation is the same for the root bending moments. The tails are obviously deflecting toward the region between the twin tail resulting in the increase of the pressure in this region, as has been observed in Fig. 5, and the forward motion of the vortex-breakdown locations on the wing surface.

Inboard Location of Twin Tail (33% wing span):
Initial Conditions:

In this case the twin tail have been moved laterally inboard with a separation distance of 33% of the

wing span. The initial conditions have been obtained after 4,000 time steps with the twin tail kept rigid. Figures 12 and 13 show the three-dimensional views and the cross-flow plane views at $x = 1.133$. It is observed that the twin tail cut through the vortex-breakdown flow splitting it into two vortical flows at each tail, with two vortical flows inside the region between the twin tail and one vortical flow outside of each tail. The vortical flows inside the region are larger but weaker than those outside of the twin tail. The flow is more symmetric in comparison with that of the initial conditions of the mid-span position. The static pressures on the inside surfaces of the twin tail are larger than those on the outside surfaces of the twin tail.

Uncoupled Bending-Torsion Twin Tail Response:

Using the same aeroelastic modulii as those of the mid-span case, the problem is solved for the uncoupled bending-torsion twin-tail response. Figures 14-21 show the fluid flow and structural responses of the this case. Figures 14 and 15 show the three dimensional views and the cross-flow plane views at $x = 1.133$ after $it = 6,000$ time steps (6 time units). It is observed that the vortex-breakdown locations on the wing have moved forward of the vortex-breakdown locations of the initial conditions. The static pressure on the inside surfaces of the twin tail are lower than those of the outside surfaces. The vortical flow in the region between the twin tail becomes stronger and larger than that of the initial conditions of Fig. 13.

The structural responses of the twin tail are given in Figs. 16-21. In Figs. 16 and 17, it is observed that the bending deflections are in the first and second mode shapes while the torsional deflections are in the first, second and third mode shapes. Here, the bending deflections show positive and negative signs and so are the torsion deflections. The maximum bending deflections are almost 50% those of the mid-span position case, and the maximum torsion deflections are 50% higher than those of the mid-span position case (compare with Figs. 6 and 7). The time history of the bending and torsion deflections and loads for the twin tail tips and mid point show the same trend of lower bending deflections and higher torsion deflections in comparison with the mid-span position case. However, within the com-

putational time used, both bending and torsion deflection are showing growth with time. Figure 20 and 21 show the total deflection distribution along the vertical distance z every 1000 time steps and the time history of the root bending moment. It is observed that the maximum total deflections of this case is 50% lower than that of the mid-span position case and similar conclusion is applicable to the root bending moment.

CONCLUDING REMARKS

The buffet response of the twin-tail configuration of the F/A-18 aircraft has been investigated computationally using three sets of equations for the aerodynamic loads, the bending and torsional deflections and the grid displacements due to the twin tail deflections. The leading-edge vortex breakdown flow has been generated using a $76°$-swept back sharp-edged delta wing which is pitched at $32°$ angle of attack. The twin tail is cantilevered at a trailing edge extension of the delta wing. Two spanwise separation distances between the twin tail are considered in this study; the midspan location with 56% spanwise separation distance and the inboard location with 33% spanwise separation distance. Only, uncoupled bending-torsion response cases are considered in this study.

For both cases of the spanwise separation distances, the locations of vortex breakdown of the wing leading-edge cores were forward of the wing trailing edge. For the midspan location case, the vortex-breakdown flow was inside the region between the twin tail. For the inboard location case, the vortex-breakdown flow was split by the twin tail into a vortical flow between the twin tail and another vortical flow outside the twin tail. In both cases, the vortex-breakdown location on the wing moved forward due to the twin tail deflections. For the mid-span location case, the bending deflections were about 50% higher than those of the inboard location case, but the torsion deflections were 50% lower than those of the inboard case. For the mid-span location case the bending deflection for each tail has the same sign; negative for the right tail and positive for the left tail. For the inboard location case, the bending deflection for each tail changed sign as the oscillations continued. The bending oscillations of the mid-span location case were in the first mode shape while those of the inboard location case were in the first

6

and second mode shapes. The torsional oscillations for both cases were in the first, second and third mode shapes.

Although many of the features of the experimental data of Washburn, et. al. were captured by this model, the results of the maximum total deflections of this study shows that the mid-span location case produces larger deflections than those of the inboard location case; opposite to those of experimental data of Washburn, et. al. results. However, ons has to remember that the computational solution is for the uncoupled bending-torsion case. Moreover, the present twin-tail configuration is different from that of Washburn, et. al. In particular, our inborad location case shows that the twin tail cuts through the vortex-breakdown flow due to its dihedral angle, while Washburn, et. al. inboard location case does not show that the twin tail cuts through the vortex-breakdown flow. Washburn's inboard case has vertical twin tail with zero dihedral angle.

ACKNOWLEDGMENT

REFERENCES

1. Sellers, W. L. III, Meyers, J. F. and Hepner, T. E., "LDV Survey Over a Fighter Model at Moderate to High Angle of Attack," SAE Paper 88-1448, 1988.

2. Erickson, G. E., Hall, R. M., Banks, D. W., Del Frate, J. H., Shreiner, J. A., Hanley, R. J. and Pulley, C. T., "Experimental Investigation of the F/A-18 Vortex Flows at Subsonic Through Transonic Speeds," AIAA 89-2222, 1989.

3. Wentz, W. H., "Vortex-Fin Interaction on a Fighter Aircraft," AIAA 87-2474, AIAA Fifth Applied Aerodynamics Conference, Monterey, CA August 1987.

4. Lee, B. and Brown, D., "Wind Tunnel Studies of F/A-18 Tail Buffet," AIAA 90-1432, 1990.

5. Rao, D. M., Puram, C. K. and shah, G. H., "Vortex Control for Tail Buffet Alleviation on a twin-Tail Fighter Configuration," SAE Paper No. 89-2221, 1989.

6. Cole, S. R., Moss, S. W. and Dogget, R. V., Jr., "Some Buffet Response Characteristics of a Twin-Vertical-Tail Configuration," NASA TM-102749, October 1990.

7. Washburn, A. E., Jenkins, L. N. and Ferman, M. A., "Experimental Investigation of Vortex-Fin Interaction," AIAA 93-0050, AIAA 31st ASM, Reno, NV, January 1993.

8. Bean, D. E. and Lee, B. H. K., "Correlation of Wind Tunnel and Flight Test Data for F/A-18 Vertical Tail Buffet," AIAA 94-1800-CP, 1994

9. Kandil, O. A., Kandil, H. A. and Massey, S. J., "Simulation of Tail Buffet Using Delta Wing-Vertical Tail Configuration," AIAA 93-3688-CP, AIAA Atmospheric Flight Mechanics Conference, Monterery, CA August 1993, pp. 566-577.

10. Kandil, O. A., Massey, S. J., and Kandil, H. A., "Computations of Vortex-Breakdown Induced Tail Buffet Undergoing Bending and Torsional Vibrations," AIAA 94-1428-CP, AIAA/ASME/ASCE/ASC Structural, Structural Dynamics and Material Conference, SC April 1994, pp. 977-993.

11. Kandil, O. A., Massey, S. J. and Sheta, E. F., "Structural Dynamics/CFD Interaction for Computation of Vertical Tail Buffet," International Forum on Aeroelasticity and Structural Dynamics, Royal Aeronautical Society, Manchester, U.K., June 26-28, 1995, pp. 52.1-52.14.

12. Kandil, O. A., Sheta, E. F. and Massey, S. J., "Buffet Responses of a Vertical Tail in Vortex Breakdown Flows," AIAA 95-3464-CP, AIAA Atmospheric Flight Mechanics Conference, Baltimore, MD, Aug. 7-9, 1995, pp. 345-360.

13. Straganac, T. W., "A Numerical Model of Unsteady, Subsonic Aeroelastic Behavior," NASA Technical Memorandum 100487, December 1987.
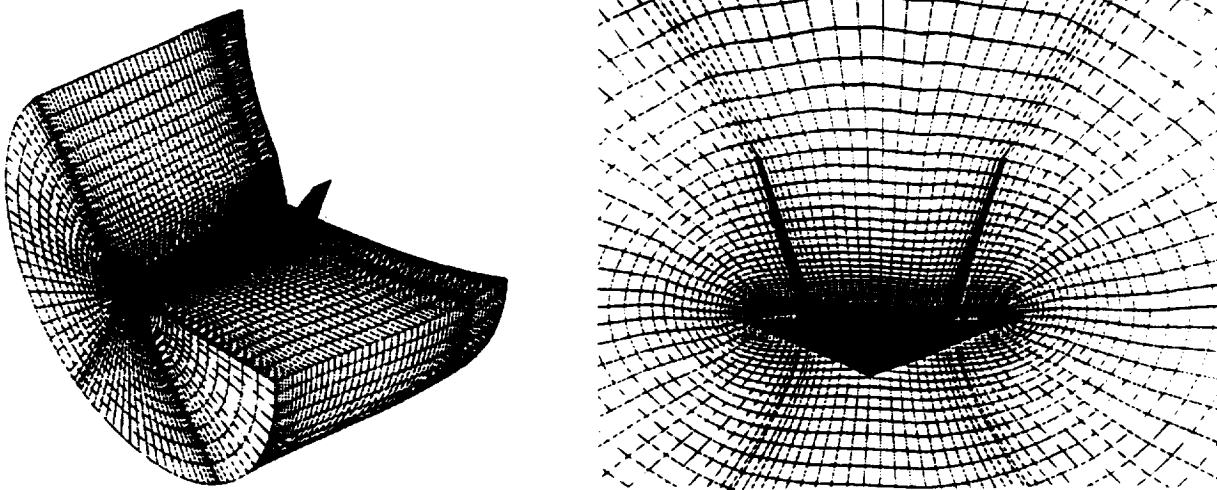
Figure 1. Three-dimensional grid topology and blow-up of the wing twin-tail configuration (The tails are in Mid-span position).
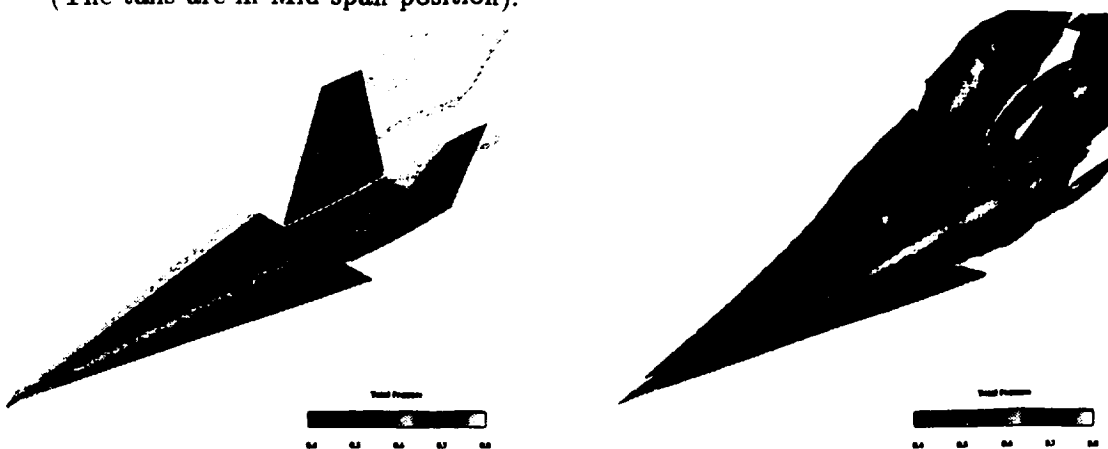

Figure 2. Three-dimensional view showing the total pressure on the surfaces, vortex-core particle traces, and vortex-core iso-total pressure surfaces, initial conditions (Mid-span position).
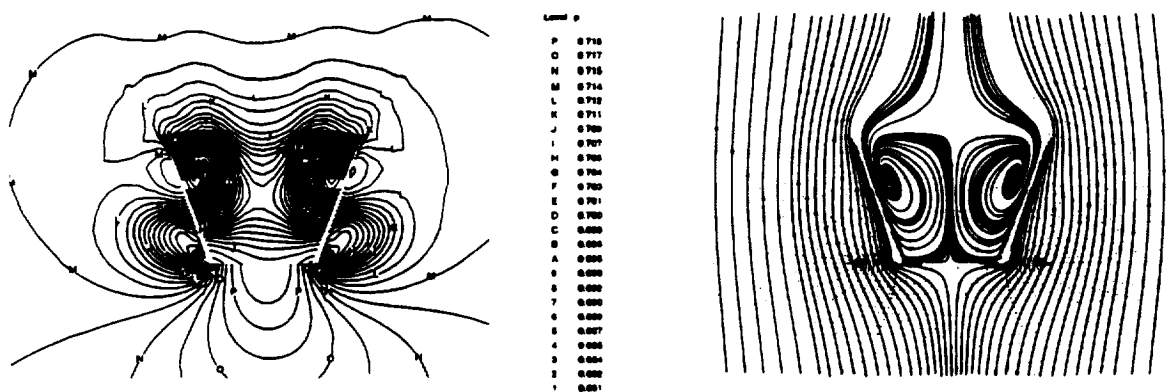

Figure 3. Initial conditions for static pressure and instantaneous streamlines in a cross-flow plane, $x = 1.133$ (Mid-span position).
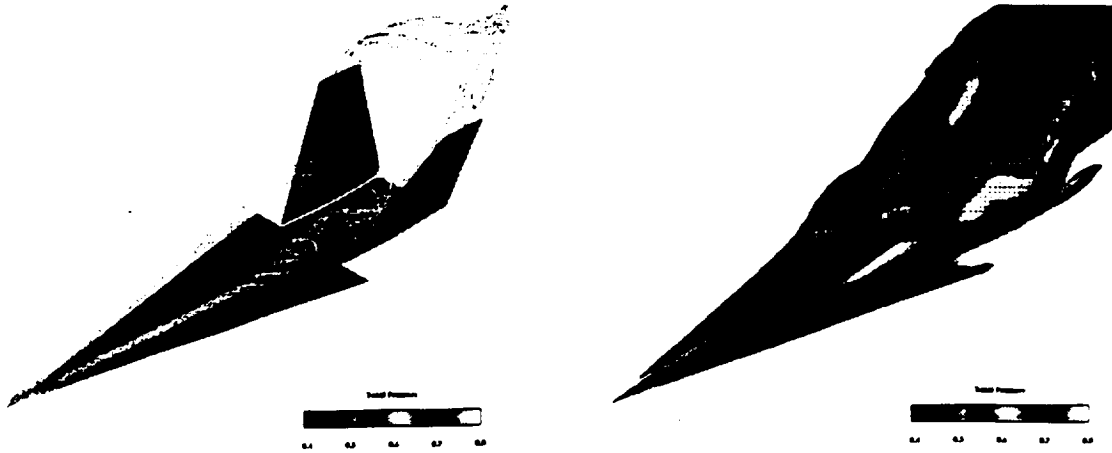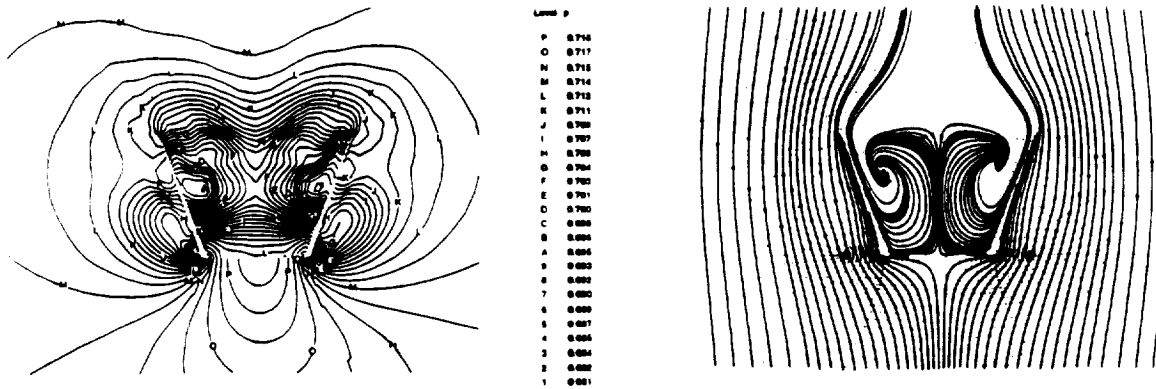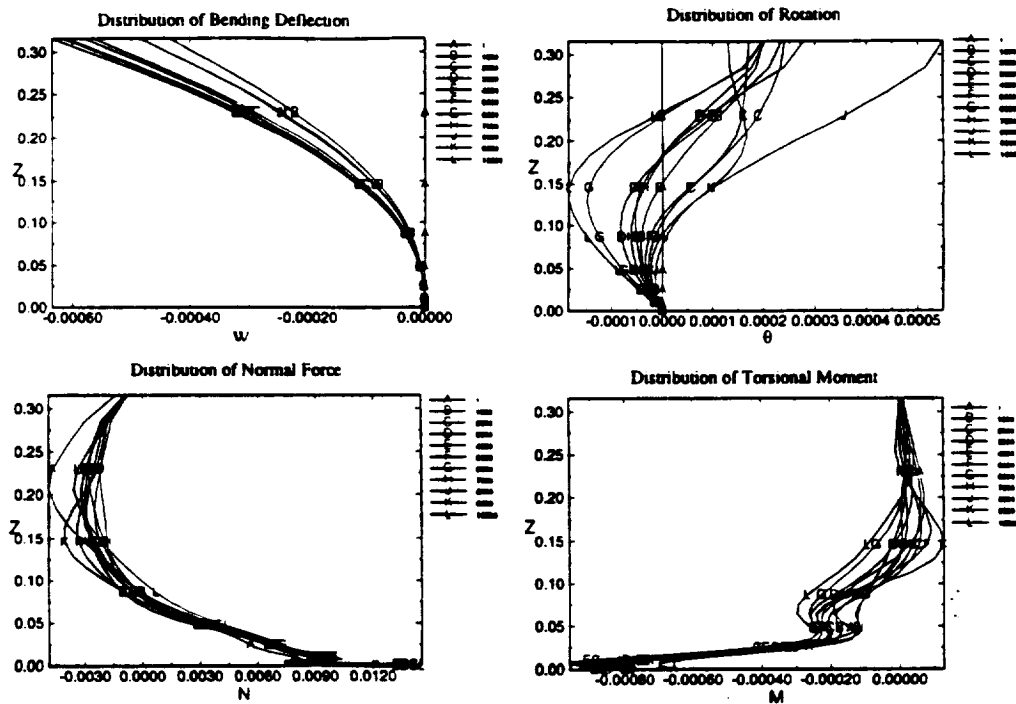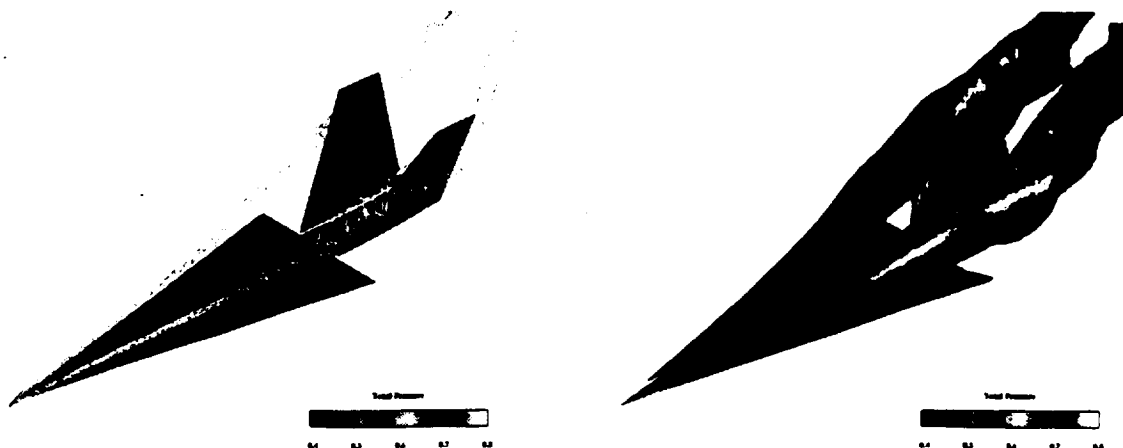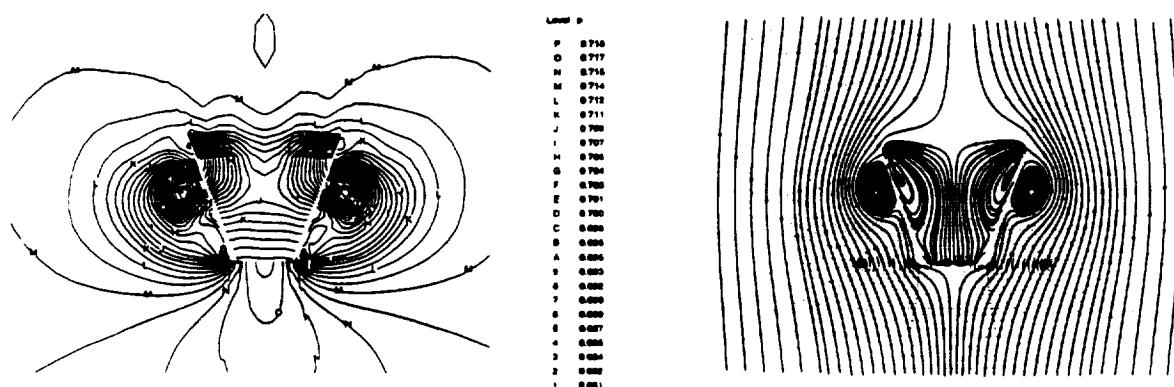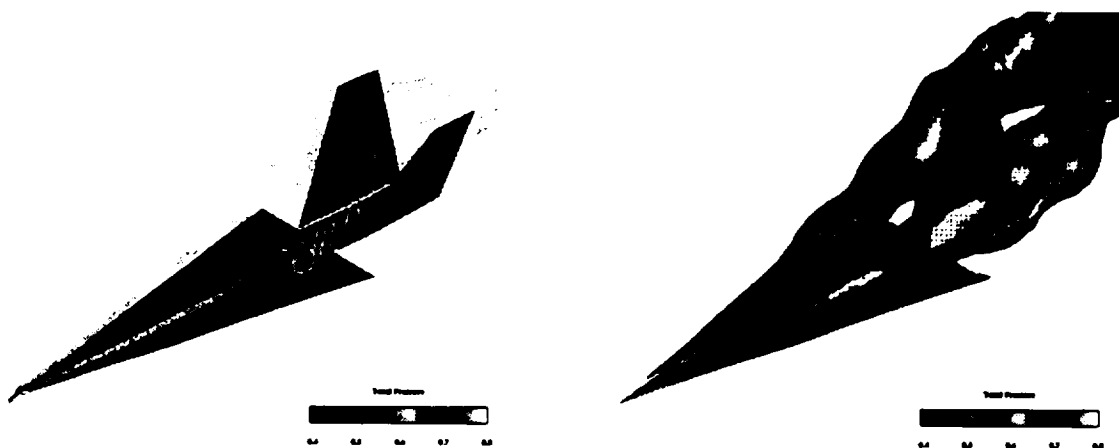
Figure 4. Three-dimensional view showing the total pressure on the surfaces, vortex-core particle traces. and vortex-core iso-total pressure surfaces after $it = 6.000$ (Mid-span position).
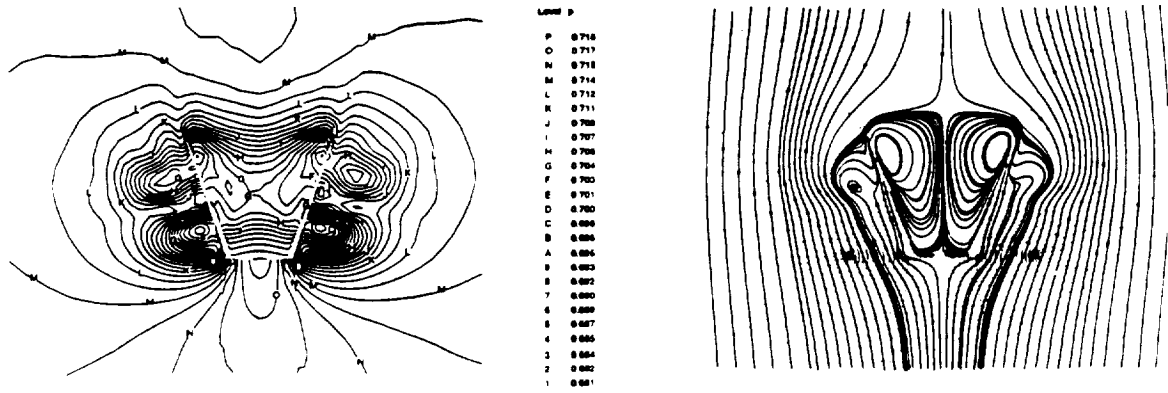

Figure 5. Snap shots of static pressure and instantaneous streamlines in a cross-flow plane, $x = 1.133$ after $it = 6.000$ (Mid-span position).
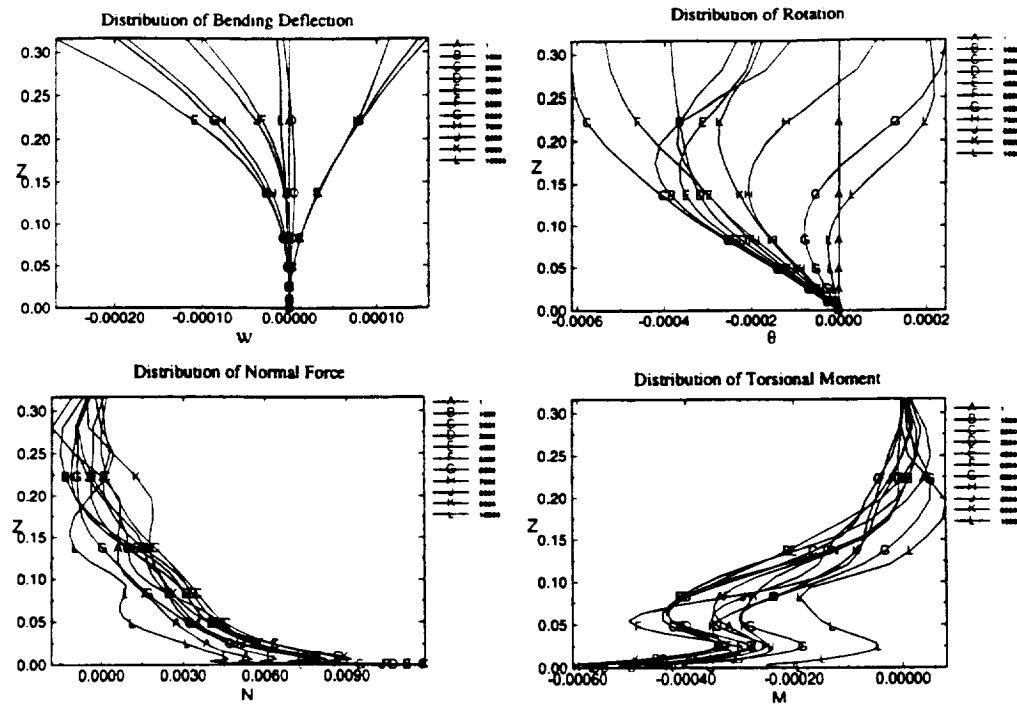

Figure 6. Distribution of the deflection and load responses for an uncoupled bending-torsion case. Right tail (Mid-span position).

9
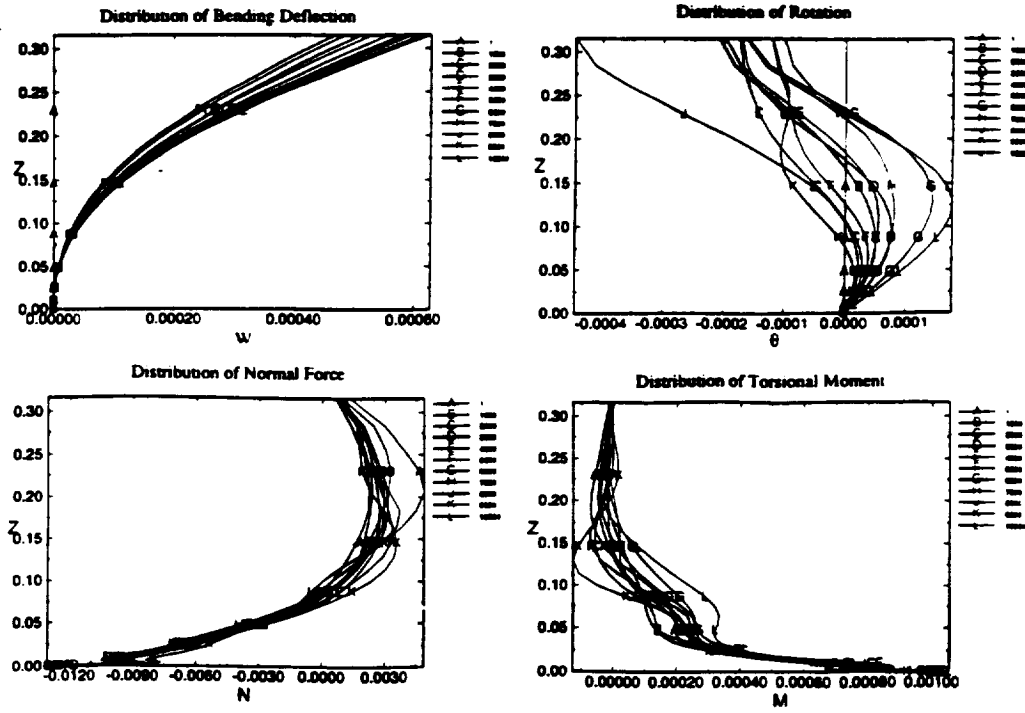
Figure 7. Distribution of the deflection and load responses for an uncoupled bending-torsion case. Left tail (Mid-span position).
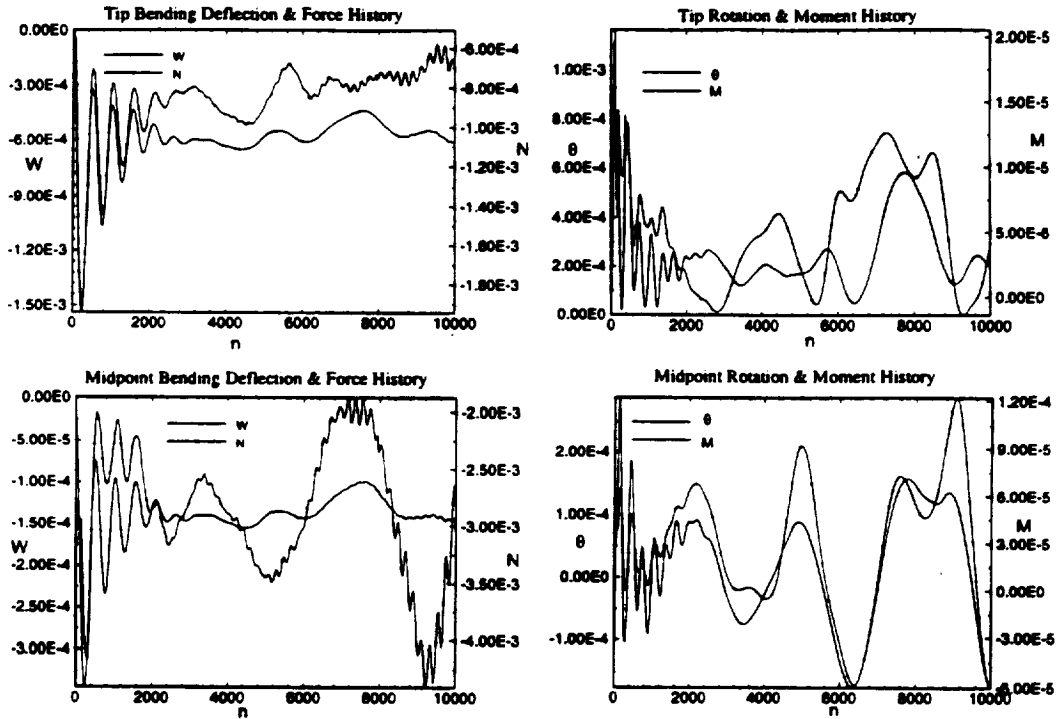
Figure 8. History of the deflection and load responses for an uncoupled bending-torsion case. Right tail (Mid-span position).
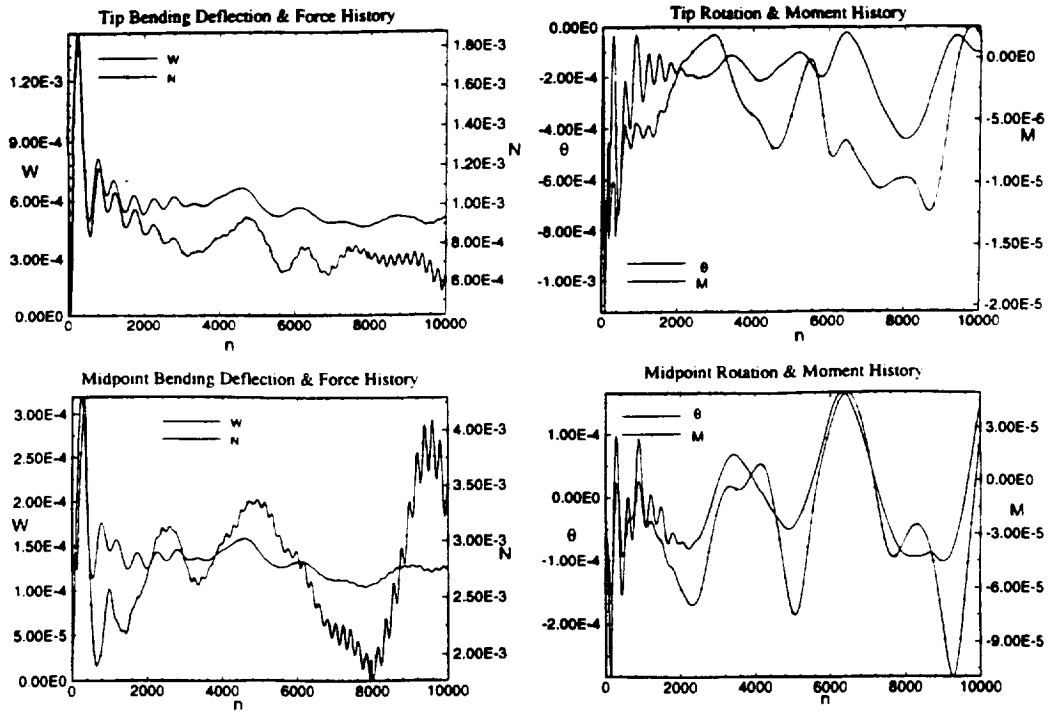
Figure 9. History of the deflection and load responses for an uncoupled bending-torsion case. Left tail (Mid-span position).
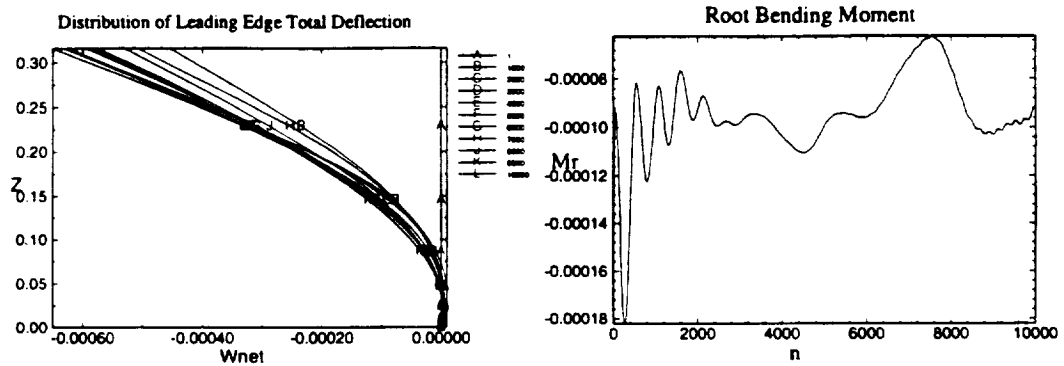
Figure 10. Total structural deflections and root bending moment. Right tail (Mid-span position).
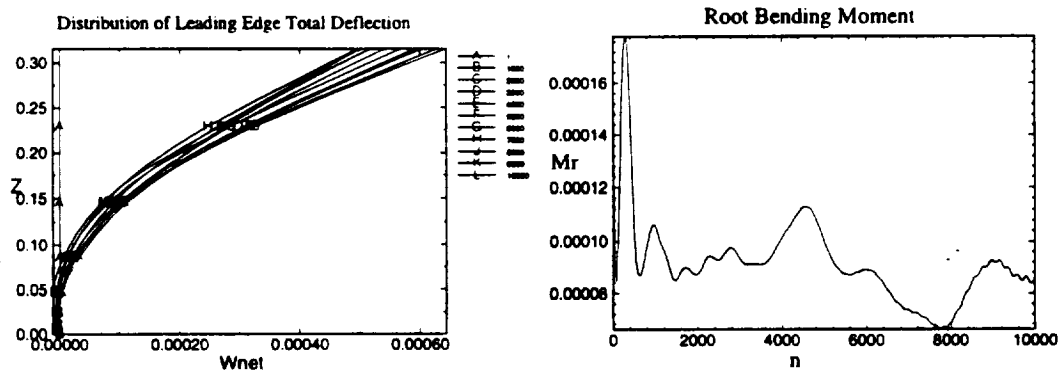
Figure 11. Total structural deflections and root bending moment. Left tail (Mid-span position).

Figure 12. Three-dimensional view showing the total pressure on the surfaces, vortex-core particle traces, and vortex-core iso-total pressure surfaces, initial conditions (Inboard position).

Figure 13. Initial conditions for static pressure and instantaneous streamlines in a cross-flow plane, $x = 1.133$ (Inboard position).

Figure 14. Three-dimensional view showing the total pressure on the surfaces, vortex-core particle traces, and vortex-core iso-total pressure surfaces after $it = 6,000$ (Inboard position).

12

Figure 15. Snap shots of static pressure and instantaneous streamlines in a cross-flow plane, $x = 1.133$ after $it = 6,000$ (Inboard position).

Figure 16. Distribution of the deflection and load responses for an uncoupled bending-torsion case. Right tail (Inboard position).
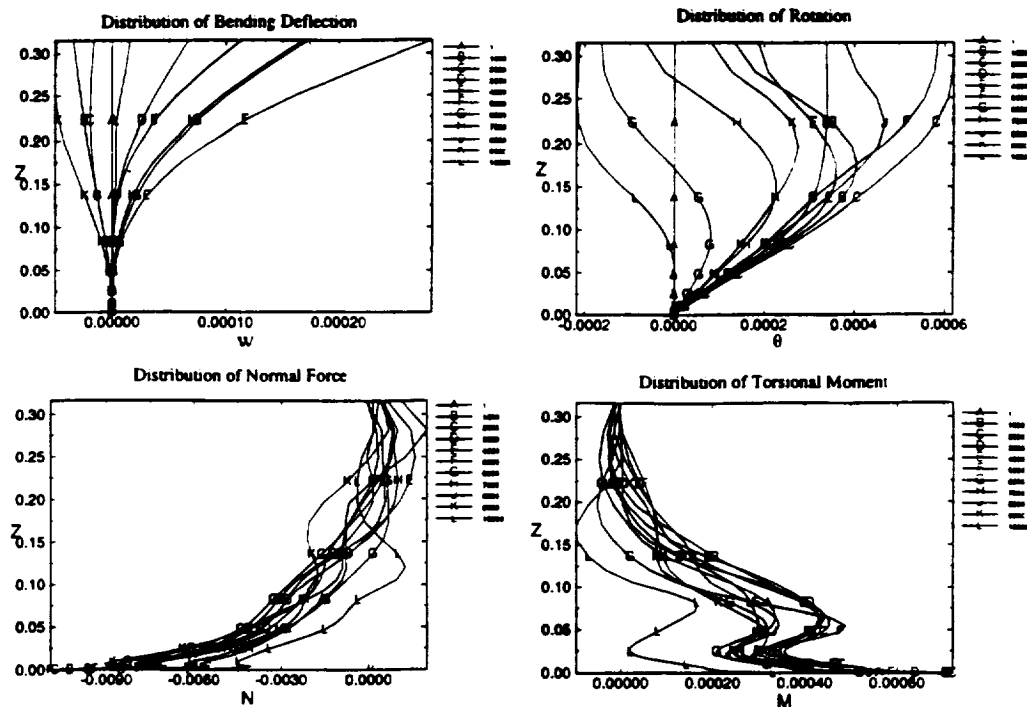
Figure 17. Distribution of the deflection and load responses for an uncoupled bending-torsion case. Left tail (Inboard position).
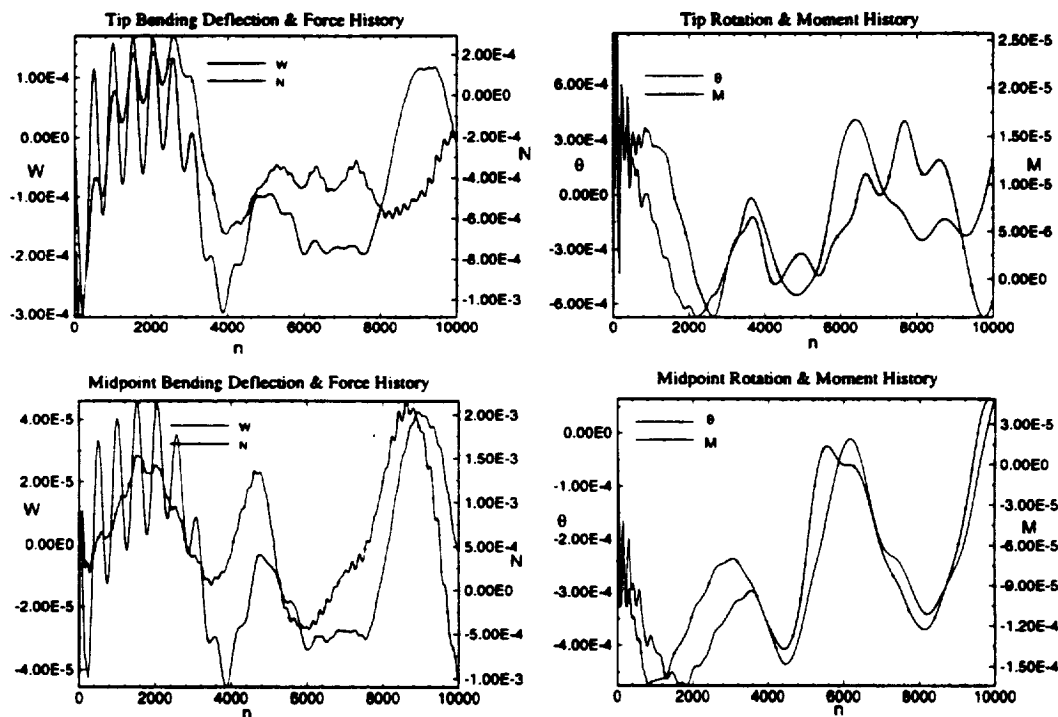

Figure 18. History of the deflection and load responses for an uncoupled bending-torsion case. Right tail (Inboard position).
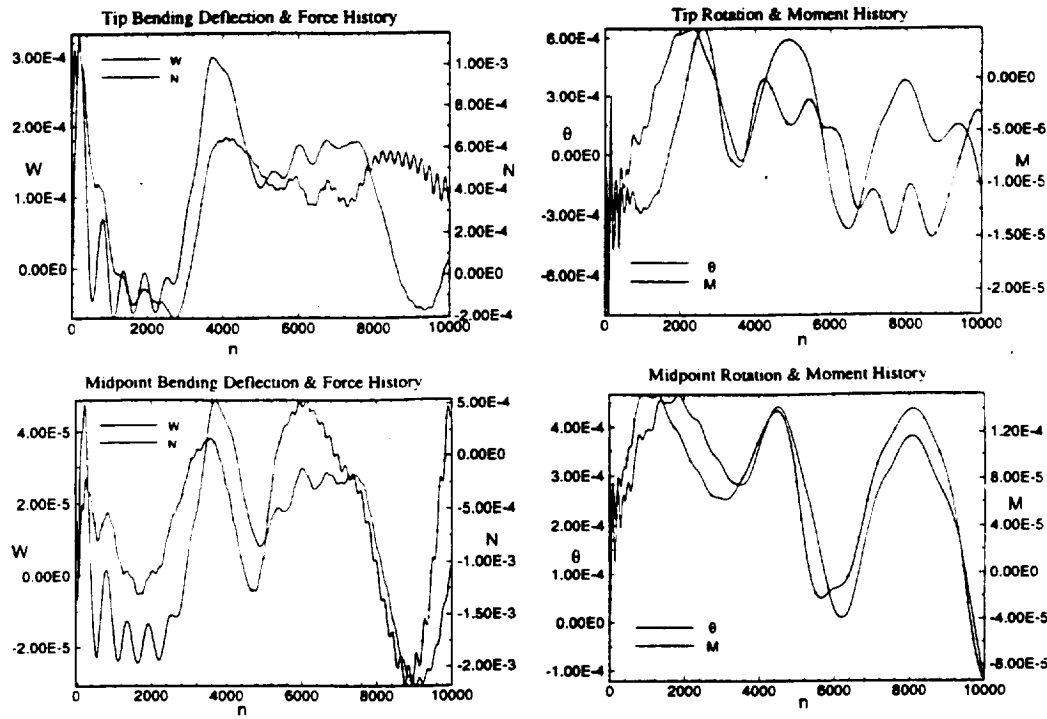
Figure 19. History of the deflection and load responses for an uncoupled bending-torsion case. Left tail (Inboard position).
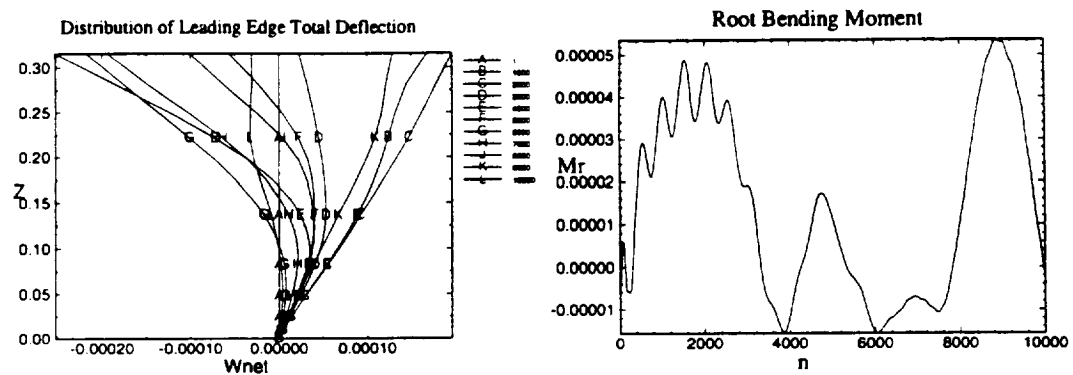
Figure 20. Total structural deflections and root bending moment. Right tail (Inboard position).
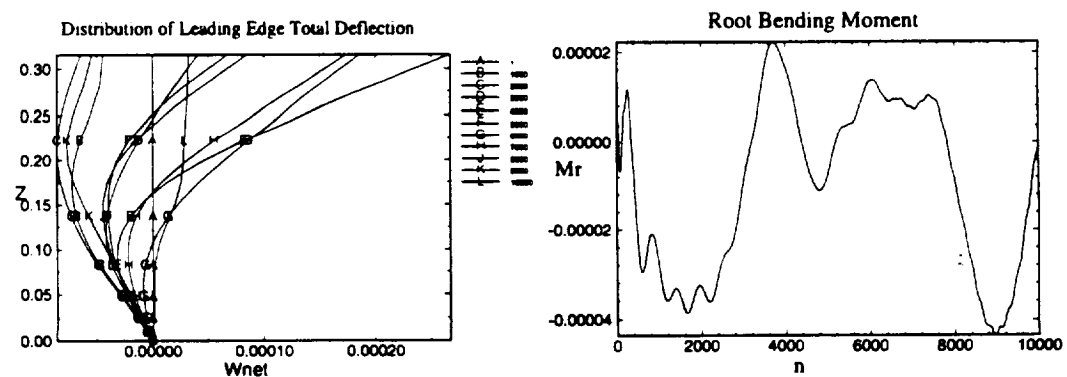
Figure 21. Total structural deflections and root bending moment. Left tail (Inboard position).